Research Article

Extraction of Cellulose Nanocrystals and Nanofibers from Rubber Leaves and Their Impacts on Natural Rubber Properties

Wanasorn Somphol, Napassorn Chanka and Tanabadee Boonmalert
Department of Chemical Engineering, Faculty of Engineering, Kasetsart University, Bangkok, Thailand

Surapich Loykulnant
National Metal and Materials Technology Center, Pathum Thani, Thailand

Paweena Prapainainar, Anusorn Seubsai and Peerapan Dittanet*
Department of Chemical Engineering, Faculty of Engineering, Center of Excellence on Petrochemical and Materials Technology, Kasetsart University, Bangkok, Thailand

* Corresponding author. E-mail: peerapan.d@ku.th   DOI: 10.14416/j.asep.2023.11.010
Received: 12 September 2023; Revised: 7 October 2023; Accepted: 17 October 2023; Published online: 27 November 2023

Abstract
This study aimed to chemically isolate two distinct types of nanocellulose derived from rubber leaves and investigate their use in natural rubber (NR). The cellulose nanocrystals (CNCs) were obtained through acid hydrolysis, while oxidation with 2, 2, 6, 6-tetramethylpiperidine-1-oxyl (TEMPO) was used to produce cellulose nanofibers (CNFs). The CNCs exhibited rigid and rod-like structures due to the removal of amorphous regions through acid hydrolysis, whereas the CNFs retained flexible, fiber-like morphologies and high aspect ratios. Incorporating CNCs or CNFs into NR improved its tensile properties, with the rigid CNCs enhancing the mechanical properties more than the flexible CNFs. CNC addition resulted in a 40% increase in tensile strength and a 38% increase in Young's modulus of NR. However, elongation at break decreased with filler content. On the other hand, CNF addition improved the elongation at the break without compromising the tensile properties. NR with CNF addition exhibited a 25% increase in tensile strength, a 30% increase in Young's modulus, and a 20% increase in elongation at break. Additionally, the biodegradability of NR nanocomposite films containing CNCs or CNFs surpassed that of unfilled NR film. Notably, a 6-month soil burial test revealed weight losses of 35% and 40% for NR nanocomposite films with CNCs and CNFs respectively, compared to a weight loss of 25% for the unfilled NR film.

Keywords: Biodegradation, Cellulose nanocrystals, Cellulose nanofibers, Natural rubber latex, Soil burial

1 Introduction

Natural rubber (NR), derived from the para rubber tree (Hevea brasiliensis), has been used in many products, such as tires, flexible tubes, medical gloves, and shoe soles [1]. The main advantageous properties of NR include high toughness, excellent flexibility, elasticity, and resilience [2]. However, the use of NR for high-performance applications is restricted by its low strength and stiffness. Therefore, the incorporation of fillers such as silica particles, carbon black, and nanocellulose into NR matrices offers several benefits in terms of enhancing mechanical properties [3], [4]. Recently, nanocellulose has gained significant attention as a reinforcing agent in NR, due to its high tensile strength, high aspect ratio, and low density [3]. The incorporation of nanocellulose into NR offers several benefits in terms of enhancing mechanical properties, barrier properties, and sustainability. The high aspect ratio of nanocellulose enables effective stress transfer

within the composite, resulting in improved strength and stiffness [5]. In addition, it has been reported that nanocellulose and the NR matrix have a strong interfacial interaction, which contributes to enhanced interfacial adhesion, reduces the potential for delamination, and improves overall durability [2]. These properties make nanocellulose a valuable additive for enhancing the mechanical performance of NR-based materials.

Nanocellulose is a biopolymer with a nanostructure derived from cellulose, one of the most abundant and renewable biopolymers. The structure of nanocellulose contains a carbohydrate macromolecule composed of polysaccharides of glucose and is made up of extremely small fibrils, typically ranging from 5–50 nm in diameter and 100 nm to several microns in length [2]. Nanocellulose has been extracted from a variety of natural sources, including wood fiber, corncobs, sugarcane bagasse, pineapple leaves, and other biomass materials [5], [6]. NR is a major agricultural crop in Thailand, and its rubber tree leaves are widely available. The rubber leaves of the rubber tree have never been used as a valuable source of nanocellulose. As a result, our research aims to maximize resource utilization while mitigating the potential environmental consequences of rubber leaf disposal.

To isolate nanocellulose from these bioresources, a range of techniques including chemical, mechanical, and enzymatic methods can be employed [3]. The selection of a particular type of nanocellulose, such as cellulose nanocrystals (CNCs) or cellulose nanofibers (CNFs), is contingent upon the isolation methods employed. Among the commonly used methods, chemical processes like acid hydrolysis and oxidative treatment are particularly prevalent in nanocellulose isolation. In the acid hydrolysis method, cellulose fibers are treated with strong mineral acids such as sulfuric acid, resulting in the breakdown of cellulose into smaller crystalline regions [7]–[9]. CNCs have a rod-like form, a high aspect ratio (length-to-diameter ratio), a large surface area, and outstanding mechanical properties. Another chemical approach involves oxidation with 2, 2, 6, 6-tetramethyl piperidine-1-oxyl (TEMPO), generating fibrillar nanoparticles or CNFs [10]. Similar to CNCs, CNFs possess a higher aspect ratio and a large surface area, contributing to their remarkable mechanical properties [11]. Due to the repulsion of carboxylate groups, cellulose nanofibers

can be easily separated in this manner. Nanocelluloses obtained through chemical methods have found extensive applications in the field of polymers. For instance, Singh *et al.*, [7] successfully extracted CNCs from red seaweed using a chemical process and combined them with PLA (polylactic acid) to enhance the properties of the polymer. Boruah *et al.*, [8] used acid hydrolysis to produce CNCs from waste paper, which improved the antifouling ability and water flux of the polyvinylidene fluoride (PVDF) membrane. By acid hydrolysis, Khatun *et al.*, [9] extracted CNCs from date palm mat fiber. The CNC rods had a diameter of 53 nm and an average length of 234 nm and were used as reinforcing agents in various industrial areas. Wang *et al.*, [12] extracted CNF from soybean using a chemical-mechanical process. CNFs had a diameter of 50 nm and a length of a micrometer.

Furthermore, nanocellulose is also fully biodegradable which can enhance the biodegradability of NR [13], [14]. Previous studies have shown that the addition of nanocellulose can expedite the breakdown of NR into simpler compounds, promoting its biodegradation in environmental settings [15]. Nanocellulose can be degraded through hydrolysis by bacteria and fungi in the soil, producing smaller oligosaccharides and monomers that can be used as carbon and energy sources by soil microorganisms [16]. For example, Supanakorn *et al.*, [16] reported that nanocomposites of NR/nanocellulose buried in soil degraded substantially over time, with a reduction in mass of up to 70% at 50% by weight of nanocellulose. In a similar work by Potivara *et al.*, [17], NR latex was subjected to microbial cultures with the incorporation of nanocellulose, leading to the complete degradation of the samples in just 6 weeks. While many researchers have explored the use of nanocellulose extracted from various biowastes as a modifier to improve the mechanical properties and biodegradability of NR, little attention has been given to the influence of nanocellulose type on the properties of NR.

This study aimed to investigate the effect of two types of nanocellulose (CNC and CNF) on the mechanical properties and biodegradability of NR. Acid hydrolysis and TEMPO oxidation were used to extract CNCs and CNFs, respectively. Electron beam vulcanization was used to harden the NR nanocomposite films. To determine the effects of nanocellulose type on the performance of NR films,

the mechanical properties, including tensile strength, elongation at break, and Young's modulus, were evaluated. Additionally, the biodegradability of NR films was investigated through a soil burial experiment over a period of 6 months, with visual observation, microscopic analysis, and weight loss measurements recorded every 3 months.

2 Materials and Methods

2.1 Materials

Natural rubber with high ammonia-concentrated latex (60% DSC) was supplied by the National Metal and Materials Technology Center (MTEC), Thailand. The mechanical stability time (MST) of latex was 138 s (ISO 35:2004). Rubber leaves were collected in southern Thailand. Other Chemicals included ethanol (AR grade, RCI Labscan, Thailand), TEMPO (2,2,6,6-tetramethylpiperidine-1-oxyl, AR grade, Sigma-Aldrich, USA), sodium hypochlorite (NaClO, AR grade, Sigma-Aldrich, USA), sodium hydroxide (NaOH, AR grade, Ajax finechem, Australia), 98% sulfuric acid (H_2SO_4, AR grade, Merck, Germany), sodium bromide (NaBr, LR, Ajax finechem, Australia).

2.2 Methods

2.2.1 Extraction of cellulose from rubber leaves

Before use, the rubber leaves were washed and dried overnight at 70 °C. Dried rubber leaves (DRL) were blended and passed through a 250-mesh sieve to obtain the powders. For waxing and bleaching, the procedures described in previous work were used [18]. the DRL powders were soaked in 10 mL of 50% v/v ethanol at 70 °C for 1 h, followed by 4% w/v NaOH at 100 °C for 2 h. After that, 1 g of the obtained sample was bleached in 20 mL of 1.7% w/v NaClO for 4 h at 90 °C. After filtration, the samples were washed and dried overnight at 70 °C. This procedure was repeated twice to produce white powders of bleached cellulose powder (BLP).

2.2.2 Extraction of CNCs by acid hydrolysis

BLP was hydrolyzed using sulfuric acid at 45 °C for 45 min at a concentration of 60% w/w, as reported previously [18]. The reaction was halted by a 10-fold excess of DI water. The resulting solution was centrifuged and dialyzed in DI water until neutral pH to remove non-cellulose and excess acid. Then, the suspension was sonicated for 30 min. Finally, the cellulose nanocrystal samples were kept in the refrigerator at 4 °C and labeled CNC.

2.2.3 Extraction of CNFs by TEMPO-mediated oxidation

1 g of BLP was mixed into 100 mL of a solution containing 1 mmol/L of TEMPO and 10 mmol/L of NaBr, as reported previously [10]. Then, 10 mmol of NaCl was added dropwise into a mixture. The pH of the mixture was maintained at 10.5 using 0.5 M of NaOH. 800 mL of ethanol was added to stop the reaction. The mixture was then centrifuged with DI water until the pH was neutralized, followed by 30 min of sonication. The suspension was kept in a refrigerator at 4 °C before use and labeled CNF.

2.2.4 Synthesis of NR/CNC and NR/CNF nanocomposite films

The CNCs were mixed with NR latex using a magnetic stirrer to achieve concentrations of 1, 2, 3, or 5% by weight relative to the rubber content. The mixture was stirred for 3 h and placed in an ultrasonic sonicator every hour to improve the nanocellulose dispersion. The solution was sealed in a plastic container with a cover to avoid solvent evaporation and then exposed directly to electron beam irradiation. All the samples were vulcanized using an 8 MeV, 200 kGy electron beam vulcanizer [19]. After that the solutions were poured into a glass mold (16.5 × 16.5 cm) and dried at 55 °C for 24 h. The resultant NR nanocomposite films were designated NR/CNC-x%, where x represented the wt% of fillers. The same procedures were prepared for NR/CNF nanocomposite films. The resultant NR nanocomposite films were designated NR/CNF-x%, where x represented the wt% of fillers.

2.3 Characterizations

Fourier transform infrared spectrometer (FTIR; Spectrum 100; PerkinElmer; USA) in the range of 600–3500 cm^{-1} was performed at a resolution of 4 cm^{-1} and 64 scans. Each sample was dried at 80 °C prior to measurement,

The crystallinity of the samples was investigated by XRD technique (Bruker; ADVANCE D8 X-ray powder diffractometer; Germany) with CuKα detector, 2θ angle range from 5–50°, a scan speed of 0.04 θ/s at 30 kV, and 30 mA. Before measurement, the CNC suspension was powdered by freeze-dried at –40 °C and 0.02 mbar. The crystallinity index (%CrI) can be determined by deconvolution Equation (1) [3].

$$\%CrI_D = (A_{cr}/A_{cr} + A_{am}) \times 100 \qquad (1)$$

where A_{cr} is the sum of the integrated area of the crystalline peaks and A_{am} is the sum of the integral area of the amorphous region.

The morphology of the CNCs and CNFs was studied by TEM (Hitachi; HT7700; Japan) and operated at an accelerating voltage of 200 kV equipped with an Eagle 4k CCD camera. The nanocellulose suspension was diluted, dropped on a copper grid surface, dyed with 2 %wt of uranyl acetate for 10 s, and washed using 50 %w/w of alcohol. Before the evaluation, the test samples were dried at room temperature.

The surface morphologies of NR nanocomposite films were analyzed by field scanning electron microscope (FE-SEM; JSM7600F; JEOL; Japan). The test was performed under secondary electron mode at an accelerating voltage of 15 kV. Before measurement, the NR nanocomposite films were sliced with liquid nitrogen and coated with a thin film of gold (Au).

The mechanical properties of NR nanocomposite films, including tensile strength, Young's modulus, and elongation at break, were investigated using a Universal Testing Machine (UTM). The samples were shaped into dumbbells per the ISO 37 (Type 2) standard method [20].

The viscoelastic properties of NR nanocomposite films were examined by a dynamic mechanical analyzer (DMA), which tested conditions at –80 to 40 °C, 5 Hz of frequency, fixed strain at 1.00%, and dynamic strain at 0.08%.

The swelling test of the NR nanocomposite films was investigated following the ASTM D471 standard method [21]. The samples were cut into 1.25 × 2.50 cm pieces with a thickness of 1 mm (weighing about 1 mg). Then, the samples were soaked in 100 mL of toluene for 24 h, after which the samples were removed, dried, and weighed. This sampling technique was repeated continuously 7 times. The swelling ratio was calculated using Equation (2):

$$Swelling\ ratio\ (Q) = M_x/M_0 \qquad (2)$$

where Q is the swelling ratio of rubber nanocomposite, M_x is the constant weight of the soaked rubber nanocomposite in toluene for x days, and M_0 is the initial weight of rubber nanocomposite. The cross-link density was calculated by Equation (3), which is the minor form of Flory-Rehner [22].

$$Cross\text{-}link\ density\ (V) = kQ^{-5/3} \qquad (3)$$

where V is the cross-link density of NR nanocomposite, k is the constant of Flory-Rehner (7.93×10^{-18}) and Q is the swelling ratio of rubber nanocomposite.

The biodegradability of NR nanocomposite films was investigated using a soil burial test to simulate the natural biodegradation. The soil was collected locally and mixed with an equal amount of organic planting soil. The soil mixture was poured to a depth of 3 cm into a plastic box. A polycarbonate net was laid down on the soil to prevent sample loss due to degradation. The samples were cut into squares 2 × 2 cm in size and buried in the soil. After that, the soil was poured to cover the samples to a depth of 12 cm from the bottom. The plastic box was placed outside in the sun, and the biodegradation test was conducted at environmental temperature during the summer season in Thailand (March-August). The humidity of the soil was maintained by spraying water on it every 2–3 days. The average temperature and relative humidity during the testing period were 30 °C and 80 %RH, recorded using a data logger (Hygrochron iBotton temperature and humidity logger). The samples were buried in the soil for 6 months. During every period of soil burial, the samples were thoroughly cleaned with water to eliminate any soil particles on the surface. The samples were air-dried at room temperature until they achieved a constant weight before being evaluated for biodegradability. The weight loss was calculated using Equation (4):

$$Weight\ loss\ (\%) = \frac{W_0 - W_1}{w_0} \times 100 \qquad (4)$$

where W_0 is the initial weight, and W_1 is the weight after being in a landfill for 3 and 6 months. The surface appearance of the samples after landfill for 3 and 6
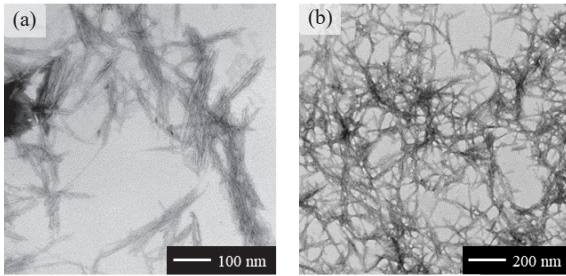
Figure 1: TEM images of (a) CNCs extracted by acid hydrolysis and (b) CNFs extracted by TEMPO oxidation.

months was investigated by SEM.

3 Results and Discussion

3.1 *Characterization of CNCs and CNFs*

3.1.1 Morphological analysis

Figure 1(a) and (b) shows the TEM images of CNCs and CNFs produced from acid hydrolysis and TEMPO oxidation, respectively. As expected, CNCs had a rod-like structure, whereas the CNFs had a fiber-like structure. CNCs had the average diameter (± standard deviation) of 12.53 ± 2.51 nm and the average length of 245.91 ± 31.44 nm, measured using the ImageJ software. The aspect ratio (L/D) was approximately 20.17 ± 3.68. CNFs had an average diameter (± standard deviation) of 10.84 ± 1.28 nm and a length that could not be precisely measured due to the entangled fibers but was estimated to be 1–2 microns. The aspect ratio (L/D) was above 100, which was much higher than CNCs. Both chemical treatments successfully fragmented the cellulose fiber bundle into nanoparticles. Thus, the diameters of individual fibers and the fibrous network are significantly reduced.

The distinct structures of CNCs and CNFs are a direct result of the specific reaction conditions employed during their production, as depicted in Figures 2 and 3. In the case of acid hydrolysis, the process involves the utilization of sulfuric acid (H_2SO_4) to break down the amorphous regions of cellulose fibers [23]. This acid treatment disrupts the hydrogen bonds that hold the cellulose chains together, with the crystalline regions being more resistant to acid hydrolysis. Consequently, the acid treatment selectively
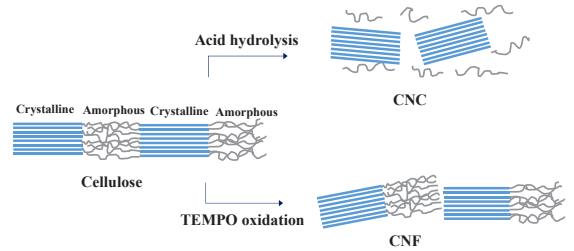

Figure 2: Schematic mechanisms of producing CNCs via acid hydrolysis and CNFs via TEMPO oxidation [23].
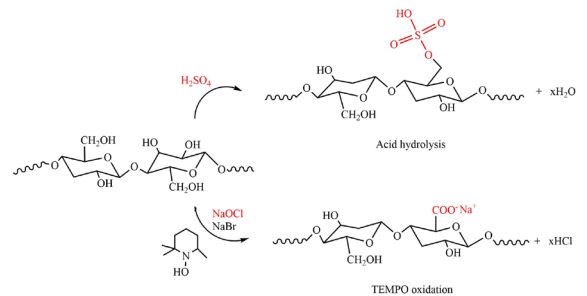

Figure 3: Chemical structures of CNCs and CNFs synthesized through acid hydrolysis and TEMPO oxidation, respectively [28].

removes the amorphous regions, leaving behind the cellulose nanocrystals with a distinctive crystal-like appearance.

On the other hand, TEMPO-oxidation involves the oxidation of cellulose using a combination of TEMPO as a radical initiator, and NaClO and NaBr as co-oxidants [24]. The primary hydroxyl groups ($-CH_2OH$) of cellulose are selectively converted into carboxylate groups during this process [25]. The incorporation of carboxyl groups introduces negative charges, which in turn increase the electrostatic repulsion between the cellulose chains, preventing them from closely packing together. Consequently, during TEMPO oxidation, cellulose is separated into individual nanofibrils or nanofiber bundles. These nanofibers exhibit a fibrous morphology, characterized by high aspect ratios and flexibility [26]. Unlike acid hydrolysis, the TEMPO oxidation method does not involve the selective removal of amorphous regions or alter the overall structure of cellulose. Instead, it chemically modifies the cellulose chains while preserving the fibrous structure, resulting in the formation of CNFs with a fiber-like morphology [27].
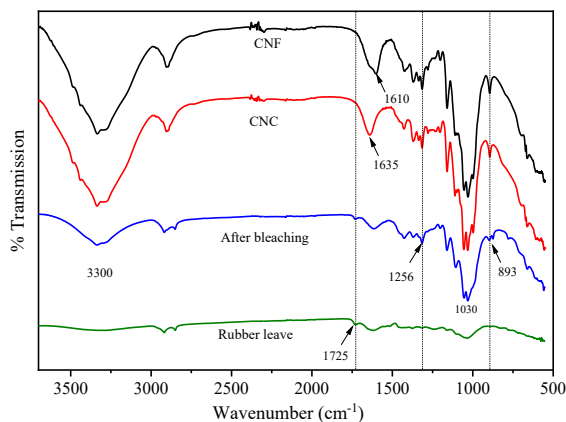
Figure 4: FTIR spectra of rubber leaf powders, bleached samples, hydrolyzed CNCs, and oxidized CNFs.

Figure 5: XRD patterns of samples following the bleaching process, hydrolyzed CNCs, and oxidized CNFs.

3.1.2 FTIR analysis

The FTIR spectra of rubber leaf powders, bleached samples, hydrolyzed CNCs, and oxidized CNFs are shown in Figure 4. All spectra exhibited broad absorption peaks at 3300–3400 and 1635 cm^{-1}, corresponding to O-H stretching and O-H bending, respectively [29]. In rubber leaf powders, -OH groups were bound by lignin, waxes, and hemicelluloses; therefore, the intensities of these peaks were broader compared to those of the beached samples, CNCs, and CNFs. After the bleaching, the intensity of these peaks was clearly visible, indicating the -OH of the cellulose. The rubber leaf powders exhibited an absorption band at 1725 cm^{-1} due to the C=O stretching of ester bonds in a ferulic acid and p-coumaric acid structure in the lignin and hemicellulose structure [18]. However, after removing lignin and hemicellulose via the bleaching process, these bands were no longer visible. CNCs and CNFs exhibited absorption bands at 1030, 893, and 1256 cm^{-1} indicating C-O stretching, C-H stretching, and CH$_2$ bending, respectively. These bands are characteristic of the cellulose structure [29]. This result demonstrated that the chemical treatment was successful in removing non-cellulose materials and synthesizing CNCs and CNFs. The prominent peak at 1610 cm^{-1} for TEMPO oxidized CNF correlated with carbonyl groups, distinguishing it from the acid hydrolyzed and bleached rubber leaf powders [30].
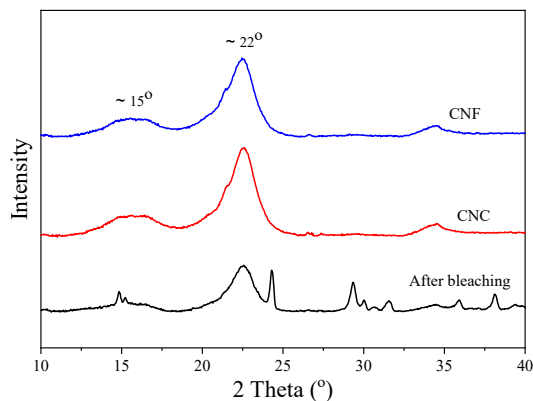
3.1.3 XRD analysis

To examine the crystalline structure of CNCs and CNFs, XRD analysis was performed, and the corresponding XRD pattern is shown in Figure 5. The XRD results revealed the presence of cellulose I peaks at approximately $2\Theta = 15°$ (1 1 0), $22°$ (0 0 2), and $34.5°$ (0 4 0) for all samples. The peaks at $2 = 15°$ and $22°$ corresponded to the amorphous and crystalline phases of cellulose I, respectively [31]. The XRD peaks of CNCs and CNFs were more distinct and pronounced compared to the samples after the bleaching process, indicating a higher degree of crystallinity. The crystallinity index (CrI_D) values of samples after bleaching, CNCs, and CNFs were determined to be 51.21%, 56.53%, and 72.71%, respectively. The highest CrI_D values were observed in CNCs, indicating a breakdown of the glycosidic bonds in cellulose, resulting in the formation of smaller cellulose fragments. Consequently, an overall increase in the crystallinity of CNCs was observed. This result further confirmed the dissolution of amorphous regions in cellulose fibers during the acid hydrolysis process [32]. In contrast, the crystallinity of CNFs did not experience a substantial increase. This is because the TEMPO oxidation method only introduced carboxyl groups and electrostatic repulsion on the cellulose chains, preventing them from closely packing together. This phenomenon resulted in the formation of nanofibrils instead of selectively destroying the amorphous regions. Therefore, the
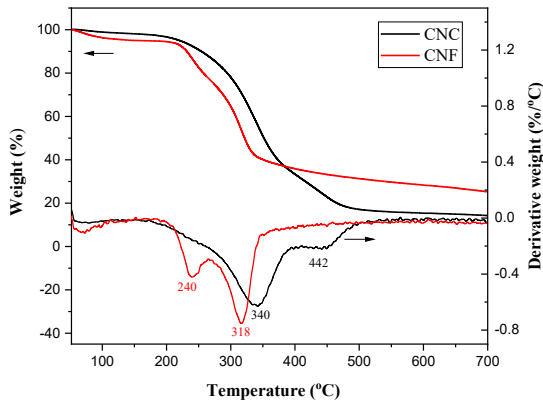
Figure 6: TGA curves of CNC and CNF samples synthesized by acid hydrolysis and by TEMPO oxidation, respectively.

fibrous structure of cellulose was preserved, resulting in the formation of CNFs with a fibrous morphology, high aspect ratios, and flexibility.

3.1.4 Thermal analysis

The thermal stability and decomposition behavior of the CNC and CNF samples were investigated using TGA analysis, as presented in Figure 6. The TGA curves displayed the weight (%) and derivative weight (%/°C) of the samples upon heating. For CNCs, the main weight loss associated with cellulose decomposition was observed at 340 °C and continued up to 450 °C. This higher decomposition temperature is due to the higher crystallinity of CNCs and the sulfonate groups formed during the acid hydrolysis process [33]. In contrast, CNFs exhibited a two-step decomposition pattern. The first decomposition step at 240 °C can be attributed to the decomposition of sodium carboxylate groups (-COONa) on the nanocellulose surface [34]. The second decomposition step appeared at 318 °C, corresponding to the degradation of cellulose structure [35]. The lower crystallinity of CNFs resulted in a slight shift towards lower decomposition temperatures compared to CNCs.

3.2 Properties of NR nanocomposite films

3.2.1 Swelling test

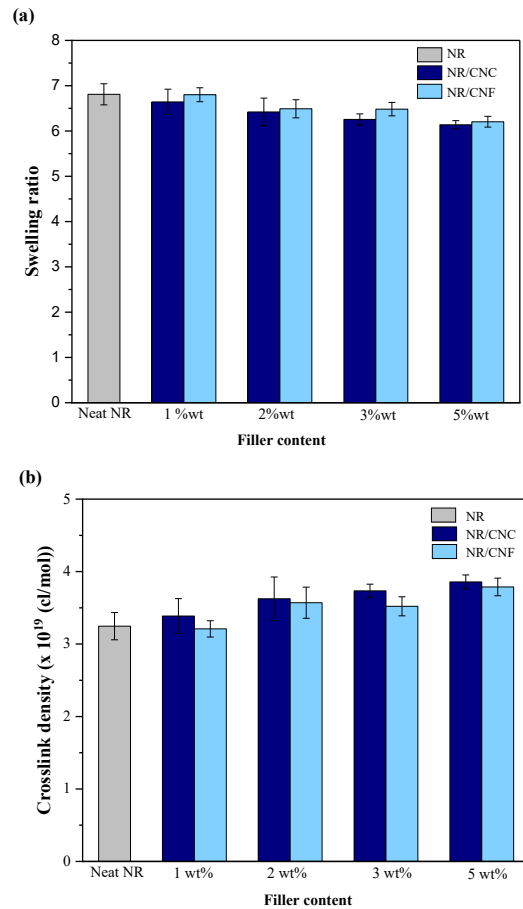The swelling ratio of natural rubber is a crucial

Figure 7: (a) Swelling ratio and (b) crosslink density of NR, NR/CNC, and NR/CNF nanocomposite films. At least five measurements were collected to calculate the mean and standard deviation.

parameter that indicates its ability to absorb a solvent. It quantifies the change in NR volume after immersion in a solvent for a specific duration. In this study, the swelling test was conducted by immersing NR films in a toluene solution for 7 days, and the corresponding swelling ratios for all samples were calculated. The cross-link density characterized by the density of chemical linkages between polymer chains in cured NR was then calculated using the Flory-Rehner equation [21]. Higher degrees of cross-linking lead to lower swelling ratios. Figure 7 displays the swelling ratio and crosslink density of all samples. Pure NR vulcanized by electron beam irradiation at 200 kGy exhibited lightly crosslinked characteristics, which

was consistent with the literature [19]. All NR/CNC and NR/CNF nanocomposite films exhibited lower swelling ratios and higher cross-linking densities compared to pure NR films. In addition, an increase in filler content had shown an impact on these properties. This finding was consistent with other researchers that the nanocellulose can enhance the crosslinking of NR [36]. During the curing process, the hydroxyl groups in nanocellulose can react with rubber molecules, resulting in the formation of additional cross-links [37]. This increased cross-linking makes it more challenging for toluene to penetrate the NR films, thereby reducing the swelling ratio and promoting higher cross-linking density. When comparing the effects of CNC and CNF addition, CNC showed slightly better performance in terms of swelling and cross-linking. However, the results of the CNC and CNF were within the standard deviation.

3.2.2 Tensile properties

Figure 8 shows the tensile properties of all nanocomposites. For the tensile strength, as shown in Figure 8(a), both NR/CNC and NR/CNF nanocomposites exhibited higher tensile strength compared to neat NR. The neat NR had a tensile strength of 12.3 MPa, which gradually increased with the addition of CNCs. The maximum tensile strength improvement of up to 40% was achieved in NR nanocomposite with the addition of 2 wt% CNCs, while for CNFs, the maximum tensile strength increase was up to 25% at 2 wt% CNFs. Similarly, the addition of CNCs and CNFs enhanced the Young's modulus of NR films, as shown in Figure 8(b). The Young's modulus of the neat NR was 0.65 MPa. The maximum Young's modulus of NR nanocomposite containing CNCs and CNFs increased by up to 38% and 30%, respectively, compared to neat NR. Comparing CNCs and CNFs, NR with CNC addition had greater tensile strength and Young's modulus than those with CNFs. This difference can be attributed to the higher crystallinity of CNCs.

It has also been reported that the addition of CNC or CNFs to NR nanocomposites improves their tensile strength and Young's modulus. Depending on the used materials and processes, the degree of improvement can vary [38], [39]. For instance, Jiang *et al.*, observed an increase in both tensile strength and Young's
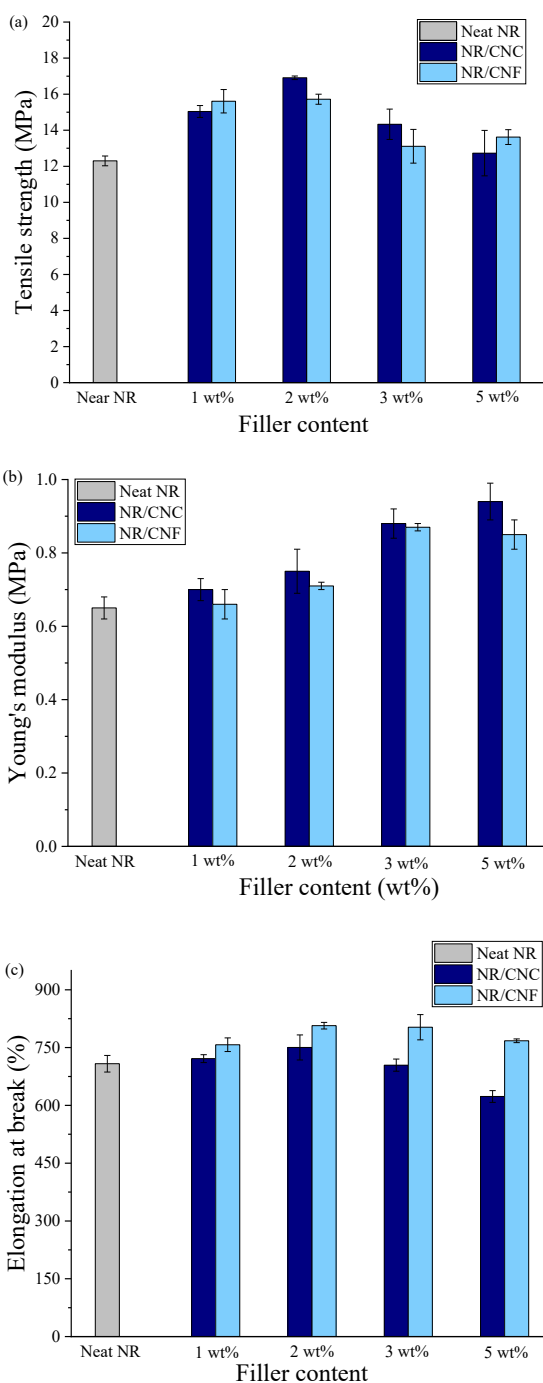

Figure 8: NR nanocomposite film mechanical properties: (a) tensile strength, (b) Young's modulus, and (c) elongation at break. At least five measurements were collected to calculate the mean and standard deviation.

modulus of NR when 5wt% of CNCs extracted from cotton via acid hydrolysis were introduced, resulting in improvements of 40% and 10%, respectively [38]. Similarly, Kumagai *et al.*, achieved enhancements in tensile strength and Young's modulus, with a 4 phr addition of CNFs obtained through alkali treatment and steam explosion, leading to improvements of 14% and 37%, respectively [39]. This improvement resulted from the large surface area for adhesion between the nanocellulose and the NR matrix, which enhanced interfacial bonding, increased crosslink density, and provided the material with greater stiffness and strength [40].

The addition of CNCs and CNFs also affected the elongation at the break of NR films, as depicted in Figure 8(c). The elongation at the break of the neat NR was 670%. The addition of up to 2 wt% of CNCs did not affect the elongation at the break of NR. However, further increasing the CNC content reduced the elongation at the break of NR nanocomposite substantially. In contrast, CNF addition led to improvement in the elongation at the break of NR nanocomposite, providing a 20% increase (at 2 wt%) compared to neat NR. Increasing CNF content did not have a substantial effect on the elongation at break and remained unchanged. This difference between CNC and CNF can be attributed to the higher aspect ratio and greater flexibility of CNFs, which provide greater elongation at break.

3.2.3 Viscoelastic properties

Figure 9 illustrates the viscoelastic properties of NR nanocomposite films analyzed using a dynamic mechanical analyzer (DMA). The DMA test was performed at temperatures ranging from –80 to 40 °C to investigate the elastic and viscous behaviors of NR during deformation. The storage modulus (E') and tan δ of the NR nanocomposite were plotted against temperature, with the peak of the tan δ representing the glass transition temperature (T_g) of the materials [41], [42]. As depicted in Figure 9(a) and (b), the viscoelastic behaviors of NR with the addition of CNCs or CNFs exhibit similarities. The addition of nanofillers leads to an increase in the E' of the NR nanocomposite. With an increase in filler content, the E' of NR nanocomposite rises consistently, consistent with the results observed in the tensile test. Both CNCs and CNFs
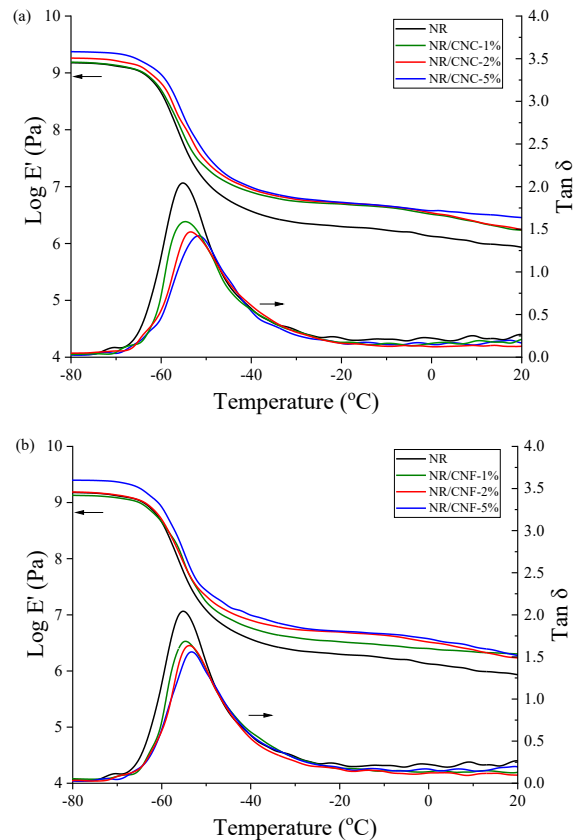

Figure 9: Storage modulus and tan δ from DMA analysis of (a) NR/CNC and (b) NR/CNF nanocomposite films.

effectively reinforce the rubber matrix, resulting in an elevated elastic modulus (stiffness) of the composite. Consequently, the material becomes more resistant to deformation and demonstrates a higher degree of elasticity.

Furthermore, CNCs and CNFs have the ability to modify the viscoelastic behavior of NR, leading to improved damping properties. An observed decrease in tan δ with increasing filler content indicates a reduction in the damping property of the NR nanocomposites [43]. This phenomenon is due to the enhanced interfacial interaction between nanofillers and the rubber matrix, which results in increased stiffness and reduced mobility of the rubber chains [44], [45]. Consequently, the ability of the materials to deform and dissipate energy is diminished, resulting in a lower tan delta peak. Additionally, the T_g of all NR
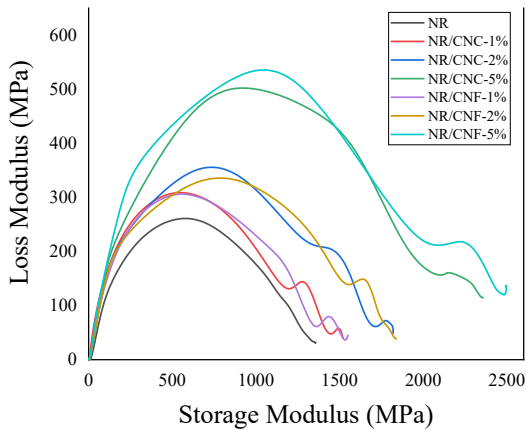
Figure 10: Cole-Cole plots of NR nanocomposites.

nanocomposites experienced a slight shift towards higher temperatures compared to unfilled NR. This shift is also attributed to alterations in the local mobility of the polymer chains induced by the interaction with the nanofillers.

The Cole-Cole plots of all NR nanocomposites are depicted in Figure 10, where the loss modulus is plotted as a function of the storage modulus. The curvature of the Cole-Cole plots has been successfully used to examine the homogeneity of polymer composites [46]–[48]. A homogeneous polymeric system displays a semicircle diagram in the Cole-Cole plot, whereas a heterogeneous polymeric system displays an imperfect semicircle diagram [48]. As shown in Figure 10, the Cole-Cole plot of pure NR was smooth and nearly semicircular. With the addition of CNCs or CNFs, however, the Cole-Cole plot of all NR nanocomposites deviated from the semicircle shape, indicating the presence of two-phase systems [47].

To determine the adhesion effectiveness of nanocellulose and NR matrix, the coefficient of effectiveness (C) was calculated using the following Equation (5) [46] :

$$C = \frac{(E'_g/(E'_r)_{NR\ nanocomposite}}{(E'_g/(E'_r)_{Pure\ NR}} \qquad (5)$$

where E'_g and E'_r represent the storage modulus in the glassy and rubbery regions, respectively. The temperature for the glassy region for pure NR and NR nanocomposite was studied at −80 °C. The C factor represents the extent to which nanocellulose

contributes effectively to the transition from a glassy to a rubbery state of the material. A lower C value suggests a more efficient dispersion of nanocellulose within the polymer matrix. Table 1 shows the calculated C values for all NR nanocomposites. In both NR/CNC and NR/CNF nanocomposites, the C value decreased as the filler content increased. This decrease indicated strong adhesion between nanocellulose and the NR matrix, which explains the enhanced tensile strength and Young's modulus of the NR/CNC and NR/CNF nanocomposites in this study [46].

Table 1: Coefficient of effectiveness (C) of NR nanocomposites

Samples	Coefficient of Effectiveness (C)
NR	1
NR/CNC-1%	0.81
NR/CNC-2%	0.74
NR/CNC-5%	0.72
NR/CNF-1%	0.79
NR/CNF-2%	0.71
NR/CNF-5%	0.70

3.2.4 Biodegradation study

The biodegradability of the NR nanocomposite films was evaluated by measuring the percentage weight loss of the samples after 3 and 6 months of soil burial. Prior to testing, the samples were cleaned with water and air-dried until a constant weight was achieved. Table 2 presents the percentage weight loss of pure NR compared to NR/CNC and NR/CNF nanocomposite films with a filler content of 2 wt%. It was observed that all NR/CNC and NR/CNF nanocomposite films exhibited higher weight loss compared to unfilled NR films. After 3 months, the unfilled NR film showed a weight loss of 8.51%, which increased to 13.49% after 6 months. The addition of CNCs accelerated the weight loss to 12.26% after 3 months and 35.37% after 6 months. Notably, the NR/CNF nanocomposite films exhibited the highest weight loss, reaching 13.49% after 3 months and 40.62% after 6 months.

The weight loss observed in all samples was accompanied by visible changes in their physical appearance. Table 3 displays visual images of the samples before and after 3 and 6 months of soil burial. A substantial color shift, from brown-yellow to dark brown, was found across all formulations of NR

nanocomposite films, which was attributed to staining from the planting soil used in the study. Prior to soil burial, the surface of each sample appeared smooth. After 3 months, the surface roughened and small cracks appeared. These cracks had expanded in size after 6 months of soil burial, and the samples showed signs of shrinkage, increased brittleness, and more prominent surface roughness.

Table 2: Weight loss (%) of NR nanocomposite films after soil burial

Samples	Weight Loss (%)	
	3 months	6 months
NR	8.51 ± 1.14	25.10 ± 6.06
NR/CNC-2%	12.26 ± 2.40	35.37 ± 5.16
NR/CNF-2%	13.49 ± 2.80	40.62 ± 0.12

Note: Three measurements were collected to calculate mean and standard deviation.

Table 3: Visual images of NR nanocomposite films before and after soil burial

Samples	After Soil Burial		
	0 month	3 months	6 months
NR			
NR/CNC-2%			
NR/CNF-2%			

Figure 11 presents SEM images of the sample surfaces before and after 3 and 6 months of soil burial. Prior to biodegradation testing, all NR nanocomposite films had uniform and smooth surfaces. After 3 months, cracks and small pores (microvoids) began to form on the rubber surfaces, and these defects became more pronounced after 6 months of soil burial. NR films with the addition of CNCs or CNFs exhibited more severe surface damage compared to unfilled NR films. Figures 11(d), (h), (i) show traces of microorganisms, particularly near the cracks, with their presence increasing over time. These microorganisms, likely spores of Actinomycetes bacteria (*Actinomycetes* spp.), are commonly found in soil [49]–[51]. In conclusion, the presence of CNCs and CNFs in the NR films facilitated biodegradation by soil bacteria and fungi.
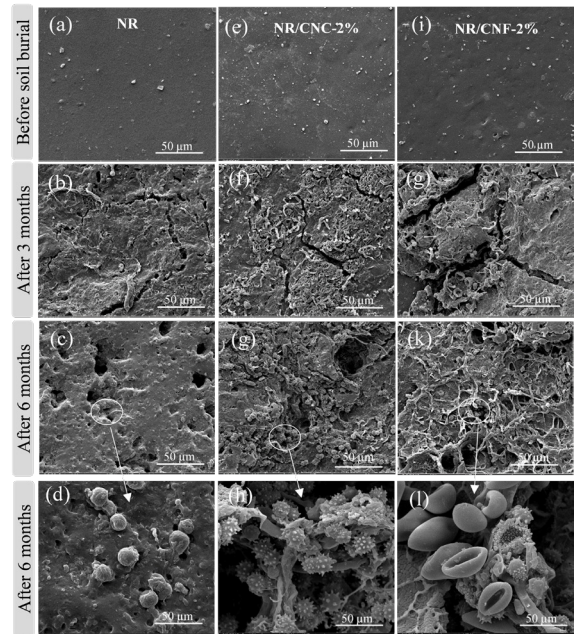

Figure 11: SEM analysis of NR nanocomposite films taken before and after soil burial for 3 and 6 months: (a)–(d) neat NR, (e)–(h) NR/CNC-2%, and (i)–(l) NR/CNF-2%.

CNF incorporation was more biodegradable than CNC incorporation. This is because CNCs, with their crystalline cellulose structures, are more resistant to decomposition than amorphous regions. On the other hand, the fibrous structure of CNFs, with more amorphous regions, allows for easier access by microbial organisms, thereby potentially enhancing their biodegradability.

4 Conclusions

CNCs and CNFs synthesized from rubber leaves were successfully used as nanofillers to improve the mechanical properties and biodegradability of NR. The different mechanisms employed in acid hydrolysis and TEMPO oxidation contributed to the distinct morphologies and properties of CNCs and CNFs. CNCs exhibited a crystal-like appearance due to the selective removal of amorphous regions, exposing the highly ordered cellulose chains. In contrast, CNFs retained their fibrous structure and high aspect ratios, facilitated by the repulsion forces generated during TEMPO oxidation. The higher crystallinity and the

presence of sulfonate groups in CNCs contribute to their higher decomposition temperature compared to CNFs, which exhibit slightly lower crystallinity. Both CNCs and CNFs enhanced the mechanical properties of NR composites. However, the differences in their morphological characteristics and interfacial interactions led to variations in the elongation at break. CNCs, with their higher crystallinity and ability to form efficient networks, exhibited greater stiffness and improved viscoelastic performance compared to CNFs. On the other hand, CNFs, with their presence of amorphous regions and lower crystallinity, enhanced the elongation at the break of NR better than CNCs. Additionally, the incorporation of CNCs and CNFs significantly influenced the biodegradability of NR under soil burial conditions. The addition of CNFs resulted in a maximum weight loss of up to 40% in NR films after 6 months of soil burial, while CNCs led to a maximum weight loss of up to 35%. In comparison, the unfilled NR films experienced a weight loss of 25%. These results highlighted the potential of utilizing rubber tree leaves as an abundant and accessible source for nanocellulose extraction. These nanocellulose materials, when incorporated into natural rubber, can serve as modifiers to enhance its properties, aligning with sustainable practices.

Acknowledgments

Author Contributions

W.S.: data analysis, investigation, writing, and methodology; N.C.: research design and data analysis; T.B.: methodology and data analysis; S.L.: conceptualization and research design; P.P.: conceptualization and data analysis; A.S.: conceptualization and data analysis; P.D.: conceptualization, data analysis, funding acquisition, project administration, writing—reviewing and editing. All authors have read and agreed to the published version of the manuscript.

Conflicts of Interest

The authors declare no conflict of interest.

References

[1] K. Cornish and S. Cherian, "Commonalities and complexities in rubber biosynthesis," in *Chemistry, Manufacture and Applications of Natural Rubber*, S. Kohjiya, Y. Ikeda, Eds. Cambridge: Woodhead Publishing, pp. 23–50, 2021.

[2] M. R. B. Mermet-Guyennet, J. d. C. Gianfelice, H. S. Varol, M. Habibi, B. Hosseinkhani, N. Martzel, R. Sprik, M. M. Denn, A. Zaccone, and S. H. Parekh, "Size-dependent reinforcement of composite rubbers," *Polymer*, vol. 73, pp. 170–173, Sep. 2015, doi: 10.1016/j.polymer.2015.07.041.

[3] K. J. Nagarajan, N. R. Ramanujam, M. R. Sanjay, S. Siengchin, B. Surya Rajan, K. Sathick Basha, P. Madhu, and G. R. Raghav, "A comprehensive review on cellulose nanocrystals and cellulose nanofibers: Pretreatment, preparation, and characterization," *Polymer Composite*, vol. 42, pp. 1588–1630, Jan. 2021, doi: 10.1002/pc.25929.

[4] M. E. Hoque, A. M. Rayhan, and S. I. Shaily, "Natural fiber-based green composites: Processing, properties and biomedical applications," *Applied Science Engineering Progress*, vol. 14, pp. 689–718, Oct. 2021, doi: 10.14416/j.asep.2021.09.005.

[5] A. A. B. Omran, A. A. B. A. Mohammed, S. M. Sapuan, R. A. Ilyas, M. R. M. Asyraf, S. S. R. Koloor, and M. Petru, "Micro- and nanocellulose in polymer composite materials: A review," *Polymers*, vol. 13, no. 231, Jan. 2021, doi: 10.3390/polym13020231.

[6] N. A. Azra, A. Atiqah, H. Fadhlina, M. A. Bakar, A. Jalar, R. A. Ilyas, J. Naveen, F. A. Sabaruddin, K. K. Lim, and M. Asrofi, "Oil-palm based nanocellulose reinforced thermoplastic polyurethane for plastic encapsulation of biomedical sensor devices: Water absorption, thickness swelling and density properties," *Applied Science Engineering Progress*, vol. 16, Feb. 2023, Art. no. 5696, doi: 10.14416/j.asep.

2022.02.001.

[7]   S. Singh, K. K. Gaikwad, and Y. S. Lee, "Antimicrobial and antioxidant properties of polyvinyl alcohol bio composite films containing seaweed extracted cellulose nano-crystal and basil leaves extract," *International Journal Biological Macromecults*, vol. 107, pp. 1879–1887, Feb. 2018, doi: 10.1016/j.ijbiomac. 2017.10.057.

[8]   P. Boruah, R. Gupta, and V. Katiyar, "Fabrication of cellulose nanocrystal (CNC) from waste paper for developing antifouling and high-performance polyvinylidene fluoride (PVDF) membrane for water purification," *Carbohydrate Polymer Technologies and Applications*, vol. 5, Jun. 2023, Art. no. 100309, doi: 10.1016/j.carpta.2023. 100309.

[9]   A. Khatun, S. Sultana, Z. Islam, M. S. Kabir, M. S. Hossain, H. P. Nur, and A. M. S. Chowdhury, "Extraction of crystalline nanocellulose (CNC) from date palm mat fibers and its application in the production of nanocomposites with polyvinyl alcohol and polyvinylpyrrolidone blended films," *Results in Engineering*, vol. 17, Mar. 2023, Art. no. 101031, doi: 10.1016/j.rineng.2023.101031.

[10] T. Saito, S. Kimura, Y. Nishiyama, and A. Isogai, "Cellulose nanofibers prepared by TEMPO-Mediated oxidation of native cellulose," *Biomacromolecules*, vol. 8, pp. 2485–2491, Jul. 2007, doi: 10.1021/bm0703970.

[11] Z. Tang, W. Li, Z. Lin, H. Xiao, Q. Miao, L. Huang, L. Chen, and H. Wu, "TEMPO-Oxidized cellulose with high degree of oxidation," *Polymers*, vol. 9, no. 421, Sep. 2017, doi: 10.3390/polym9090421.

[12] L. Wang, Q. Cui, S. Pan, Y. Li, Y. Jin, H. Yang, T. Li, and Q. Zhang, "Facile isolation of cellulose nanofibers from soybean residue," *Carbohydrate Polymer Technologies and Applications*, vol. 2, Dec. 2021, Art. no. 100172, doi: 10.1016/j.carpta. 2021.100172.

[13] J. Bras, M. L. Hassan, and C. Bruzesse, "Mechanical, barrier, and biodegradability properties of bagasse cellulose whiskers reinforced natural rubber nanocomposites," *Industrial Crops and Products*, vol. 32, pp. 627–633, Nov. 2010, doi: 10.1016/j.indcrop.2010.07.018.

[14] M. A. Misman and A. R. Azura, "Overview on the potential of biodegradable natural rubber latex gloves for commercialization," *Advanced Material Research*, vol. 844, pp. 486–489, Nov. 2013, doi: 10.4028/www.scientific.net/AMR. 844.486.

[15] C. Li, F. Huang, F. Wang, X. Liang, S. Huang, and J. Gu, "Effects of partial replacement of carbon black with nanocrystalline cellulose on properties of natural rubber nanocomposites," *Journal of Polymer Engineering*, vol. 38, pp. 137–146, Apr. 2018, doi: 10.1515/polyeng-2016-0382.

[16] G. Supanakorn, S. Taokaew, and M. Phisalaphong, "Ternary composite films of natural rubber, cellulose microfiber, and carboxymethyl cellulose for excellent mechanical properties, biodegradability and chemical resistance," Cellulose, vol. 28, pp. 8553–8566, Jul. 2021, doi: 10.1007/s10570-021-04082-4.

[17] K. Potivara and M. Phisalaphong, "Development and characterization of bacterial cellulose reinforced with natural rubber," *Materials*, vol. 12, p. 2323, Jul. 2019, doi:10.3390/ma12142323.

[18] W. Somphol, P. Prapainainar, P. Sae-Oui, S. Loykulnant, and P. Dittanet, "Extraction of nanocellulose from dried rubber tree leaves by acid hydrolysis," *Material Science Forum*, vol. 936, pp. 37–41, Oct. 2019, doi: 10.4028/www.scientific. net/MSF.936.37.

[19] C. Sukthawon, P. Dittanet, P. Saeoui, S. Loykulnant, and P. Prapainainar, "Electron beam irradiation crosslinked chitosan/natural rubber -latex film: Preparation and characterization," *Radiation Physics and Chemistry*, vol. 177, Dec. 2020, Art. no. 109159, doi: 10.1016/j.radphyschem. 2020.109159.

[20] *ISO for Rubber, Vulcanized or Thermoplastic-Determination of Tensile Stress-Strain Properties*, ISO 37, Nov. 2017.

[21] *ASTM standard for Standard Test Method for Rubber Property-Effect of Liquids*, ASTM D471, Jun. 2021.

[22] K. L. A. Cimatu, T. D. Ambagaspitiya, U. I. Premadasa, N. M. Adhikari, A. Kruse, E. Robertson, S. Guan, L. Rong, R. Advincula, and B. J. Bythell, "Polymer-solvent interaction and conformational changes at a molecular level: Implication to solvent-assisted deformation and aggregation at the polymer surface," vol. 616, pp. 221–233, Jun. 2022, doi: 10.1016/j.jcis.2022.02.006.

[23] I. Filipova, F. Serra, Q. Tarres, P. Mutje, and M. Delgado-Aguilar, "Oxidative treatments for cellulose nanofibers production: A comparative study between TEMPO-mediated and ammonium persulfate oxidation," *Cellulose*, vol. 27, pp. 10671–10688, Mar. 2020, doi: 10.1007/s10570-020-03089-7.

[24] H. Xu, J. L. Sanchez-salvador, A. Balea, A. Blanco, and C. Negro, "Optimization of reagent consumption in TEMPO-mediated oxidation of Eucalyptus cellulose to obtain cellulose nanofibers," *Cellulose*, vol. 29, pp. 6611–6627, Jun. 2022, doi: 10.1007/s10570-022-04672-w.

[25] A. Isogai, T. Saito, and H. Fukuzumi, "TEMPO-oxidized cellulose nanofibers," *Nanoscale*, vol. 3, pp. 71–85, Jan. 2011, doi: 10.1039/C0NR00583E.

[26] A. Isogai and Y. Zhou, "Diverse nanocelluloses prepared from TEMPO-oxidized wood cellulose fibers: Nanonetworks, nanofibers, and nanocrystals," *Current Opinion Solid State and Materials Science*, vol. 23, pp. 101–106, Apr. 2019, doi: 10.1016/j.cossms.2019.01.001.

[27] Y. Habibi, "Key advances in the chemical modification of nanocelluloses," *Chemical Society Reviews*, vol. 43, pp. 1519–1542, Mar. 2014, doi: 10.1039/C3CS60204D.

[28] H. C. Chen, Y. C. Huang, C. H. Wu, R. J. Jeng, and F. C. Chang, "Stable emulsion of cationic waterborne polyurethanes with cellulose nanocrystals for enhanced nanocomposite performance," *Cellulose*, vol. 30, pp. 2217–2234, Jan. 2023, doi: 10.1007/s10570-022-04989-6.

[29] T. Sukprom, S. Chanklang, S. Roddecha, C. Niamnuy, P. Prapainainar, and A. Seubsai, "Lead ions removal using pineapple leaf-based modified celluloses," *Applied Science Engineering Progress*, vol. 16, Apr. 2023, Art. no. 6002, doi: 10.14416/j.asep.2022.05.009.

[30] N. Rambabu, S. Panthapulakkal, M. Sain, and A. K. Dalai, "Production of nanocellulose fibers from pinecone biomass: Evaluation and optimization of chemical and mechanical treatment conditions on mechanical properties of nanocellulose films," *Industrial Crops and Products*, vol. 83, pp. 746–754, May 2016.

[31] N. Chanka, W. Mondach, P. Dittanet, S. Roddecha, C. Niamnuy, P. Prapainainar, and A. Seubsai, "Modification of pineapple leaf fibers with aminosilanes as adsorbents for H$_2$S removal," *Chemosphere*, vol. 266, Mar. 2021, Art. no. 129000, doi: 10.1016/j.indcrop.2015.11.083.

[32] C. Liu, B. Li, and H. Du, "Properties of nanocellulose isolated from corncob residue using sulfuric acid, formic acid, oxidative and mechanical methods," *Carbohydrate Polymers*, vol. 151, pp. 716–724, Oct. 2016, doi: 10.1016/j.carbpol.2016.06.025.

[33] F. Ghaemi, A. L. Chuah, H. Kargarzadeh, M. M. Abdi, N. F. W. M. Azli, and M. Abbasian, "Comparative study of the electrochemical, biomedical, and thermal properties of natural and synthetic nanomaterials," *Nanoscale Research Letters*, vol. 13, p. 112, Apr. 2018, doi: 10.1186/s11671-018-2508-3.

[34] B. Soni, E. B. Hassan, and B. Mahmoud, "Chemical isolation and characterization of different cellulose nanofibers from cotton stalks," *Carbohydrate Polymers*, vol. 134, pp. 581–589, Dec. 2015, doi: 10.1016/j.carbpol.2015.08.031.

[35] A. Sriruangrungkamol and W. Chonkaew, "Modification of nanocellulose membrane by impregnation method with sulfosuccinic acid for direct methanol fuel cell applications," *Polymer Bulletin*, vol. 78, pp. 3705–3728, Jul. 2021, doi: 10.1007/s00289-020-03289-y.

[36] M. Reowdecha, P. Dittanet, P. Sae-Oui, S. Loykulnant, and P. Prapainainar, "Film and latex forms of silica-reinforced natural rubber composite vulcanized using electron beam irradiation," *Heliyon*, vol. 7, Jun. 2021, Art. no. e07176, doi: 10.1016/j.heliyon.2021.e07176.

[37] E. Abraham, M. S. Thomas, and C. John, "Green nanocomposites of natural rubber/nanocellulose: Membrane transport, rheological and thermal degradation characterizations," *Industrial Crops and Products*, vol. 51, pp. 415–424, Nov. 2013, doi: 10.1016/j.indcrop.2013.09.022.

[38] W. Jiang and J. Gu, "Nanocrystalline cellulose isolated from different renewable sources to fabricate natural rubber composites with outstanding mechanical properties," *Cellulose*, vol. 27, 5801–5813, May 2020, doi: 10.1007/s10570-020-03209-3.

[39] A. Kumagai, N. Tajima, S. Iwamoto, T. Morimoto, A. Nagatani, T. Okazaki, and T. Endo, "Properties

of natural rubber reinforced with cellulose nanofibers based on fiber diameter distribution as estimated by differential centrifugal sedimentation," *International Journal of Biological Macromolecules*, vol. 121, pp. 989–995, Jan. 2019, doi: 10.1016/j.ijbiomac.2018.10.090.

[40] X. Xu, F. Liu, and L. Jiang, "Cellulose nanocrystals vs. cellulose nanofibrils: A comparative study on their microstructures and effects as polymer reinforcing agents," *ACS Applied Materials and Interfaces*, vol. 5, pp. 2999–3009, Mar. 2013, doi: 10.1021/am302624t.

[41] P. Berki, K. László, N. T. Tung, and J. Karger-Kocsis, "Natural rubber/graphene oxide nanocomposites via melt and latex compounding: Comparison at very low graphene oxide content," *Journal of Reinforced Plastics and Composites*, vol. 36, pp. 808–817, Feb. 2017, doi: 10.1177/0731684417690929.

[42] J. Liu, T. Jianxin, K. Yun, Z. Wang, and X. Sun, "Investigation of thermodynamic and shape memory properties of alumina nanoparticle-loaded graphene oxide (GO) reinforced nanocomposites," *Materials and Design*, vol. 181, Nov. 2019, Art. no. 107926, doi: 10.1016/j.matdes.2019.107926.

[43] B. Wongvasana, B. Thongnuanchan, A. Masa, H. Saito, T. Sakai, and N. Lopattananon, "Reinforcement behavior of chemically unmodified cellulose nanofiber in natural rubber nanocomposites," *Polymers*, vol. 15, p. 1274, Mar. 2023, doi: 10.3390/polym15051274.

[44] N. M. F. Hakimi, S. H. Lee, W. C. Lum, S. F. Mohamad, S. S. A. O. A. Edrus, B. D. Park, and A. Azmi, "Surface modified nanocellulose and its reinforcement in natural rubber matrix nanocomposites: A review," *Polymers*, vol. 13, p. 3241, Sep. 2021, doi: 10.3390/polym13193241.

[45] C. Correia, L. M. d. Oieira, and T. S. Valera, "The influence of bleached jute fiber filler on the properties of vulcanized natural rubber,"

[46] S. T. K. Rajan, K. J. Nagarajan, V. Balasubramani, K. Sathickbasha, M. R. Sanjay, S. Siengchin, and A. N. Balaji, "Investigation of mechanical and thermo-mechanical characteristics of silane-treated cellulose nanofibers from agricultural waste reinforced epoxy adhesive composites." *Internationl Journal of Adhesion and Adhesives*, vol. 126, Aug. 2023, Art. no. 103492, doi: 10.1016/j.ijadhadh.2023.103492.

[47] G. Fredi, A. Dorigato, M. Bortolotti, A. Pegoretti, and D. N. Bikiaris, "Mechanical and functional properties of novel biobased poly(decylene-2,5-furanoate)/carbon nanotubes nanocomposite films," *Polymers (Basel)*, vol. 12, p. 2459, Oct. 2020, doi: 10.3390/polym12112459.

[48] G. Rathinasabapathi and A. Krishnamoorthy, "Cole-cole plot of graphene nano filler disseminated glass fiber reinforced polymer composites," *Materials Today: Proceedings*, vol. 44, pp. 3816–3822, Feb. 2021, doi: 10.1016/j.matpr.2020.12.335.

[49] A. J. McCarthy and S. T. Williams, "Actinomycetes as agents of biodegradation in the environment — A review," *Gene*, vol. 115, pp. 189–192, Jun. 1992, doi: 10.1016/0378-1119(92)90558-7.

[50] A. Linos, M. M. Berekaa, and R. Reichelt, "Biodegradation of cis-1,4-polyisoprene rubbers by distinct actinomycetes: microbial strategies and detailed surface analysis," *Applied Environmental Microbiology*, vol. 66, pp. 1639–1645, Apr. 2000, doi: 10.1128/aem.66.4.1639-1645.2000.

[51] E. A. Barka, P. Vatsa, L. Sanchez, N. Gaveau-Vaillant, C. Jacquard, H. P. Klenk, C. Clément, Y. Ouhdouch, and G. P. V. Weze, "Taxonomy, physiology, and natural products of actinobacteria," *Microbiology and Molecular Biology Reviews*, vol. 80, pp. 1–43, Mar. 2016, doi: 10.1128/mmbr.00019-15.